Aerosol and Air Quality Research

ORIGINAL RESEARCH
https://doi.org/10.4209/aaqr.220108

Size-resolved Compositional Analysis and Source Apportionment of Submicron Aerosol during Lockdown Period Using HR-ToF-AMS

Special Issue:
Air Pollution and its Impact in South and Southeast Asia (VIII)

Prodip Acharja [1,2*], Akash Vispute [1,2], Prasanna Lonkar [1,2], Suresh W. Gosavi [2], Sreyashi Debnath [1,2], Narendra G. Dhangar [1], Kaushar Ali [1], Gaurav Govardhan [1,3], Sachin D. Ghude [1*]

[1] Indian Institute of Tropical Meteorology, Ministry of Earth Sciences, Pune, India
[2] Savitribai Phule Pune University, Pune 411007, India
[3] National Center for Medium Range Weather Forecasting, Ministry of Earth Sciences, Noida, U.P., India

ABSTRACT

The size-resolved compositional analysis of non-refractory submicron aerosol (NR-PM_1) was conducted using the Aerodyne High-Resolution Time-of-Flight Aerosol Mass Spectrometer (HR-ToF-AMS) instrument over Pune, India during the COVID-19 lockdown period. The aerosol composition data shows the predominant presence of organics (Org) in the mass fraction followed by sulfate, ammonium, nitrate, and chloride during the pre-lockdown and lockdown periods. The size-resolved analysis showed the unimodal size distribution of organic and inorganic constituents with peaks at 550 nm, implying the dominant presence of mixed and aged aerosol species. The stoichiometric neutralization analysis showed the almost neutralized nature of submicron aerosol with an average aerosol neutralization ratio (ANR) of 0.8. The back trajectories, cluster analysis, and potential source contribution function (PSCF) showed the industrial belt located in the western part of the study location to be the potential source regions of NR-PM_1. Positive matrix factorization (PMF) analyses have been applied to investigate the source apportionments of organic aerosols (OA). Four distinct OA factors, i.e., hydrocarbon-like OA (HOA), biomass burning OA (BBOA), low-volatile oxygenated OA (LVOOA), and semi-volatile oxygenated OA (SVOOA) were identified during the study period. Among these factors, HOA contributes nearly a quarter to the OA mass, and OOA accounted for nearly 60% of the total OA mass. The high-resolution positive matrix factorization (HR-PMF) analysis and the elemental ratios of H/C, O/C, and OM/OC showed distinct characteristics during different periods. The density of organic aerosol has been estimated using the elemental ratios and found to be 1.14, 1.28, and 1.35 respectively during the different lockdown periods, similar to 1.30 g cm^{-3} as mentioned in the literature. This study provides new insights into the chemical composition and source apportionment of the organic fraction of submicron aerosols for the first time over Pune using HR-ToF-AMS and HR-PMF.

Keywords: HR-ToF-AMS, Submicron Aerosols (NR-PM_1), High-Resolution Positive Matrix Factorization (HR-PMF), Potential Source Contribution Function (PSCF), COVID-19 lockdown

OPEN ACCESS

Received: March 1, 2022
Revised: August 8, 2022
Accepted: September 15, 2022

* **Corresponding Authors:**
Sachin D. Ghude
sachinghude@tropmet.res.in
Prodip Acharja
prodip@tropmet.res.in

Publisher:
Taiwan Association for Aerosol Research
ISSN: 1680-8584 print
ISSN: 2071-1409 online

1 INTRODUCTION

The outbreak of novel coronavirus has led to the death of millions of individuals around the world, and countries implemented strict restrictions (lockdown) to prevent the spread of the virus and preserve the health of the citizens (Dhaka *et al.*, 2020; Agarwal *et al.*, 2020). The majority of the industrial and other pollution-emitting establishments and activities, including vehicular movement, shopping malls, hotels, and construction work were closed, which caused a nearly complete cessation of anthropogenic emission of pollutants. The implemented lockdown has

ORIGINAL RESEARCH
https://doi.org/10.4209/aaqr.220108

created a unique experimental situation in India to investigate the role of anthropogenic pollution sources on air quality, which is not possible in normal conditions.

The near-complete cessation of anthropogenic activities during the lockdown periods has greatly influenced air quality over different parts of the world, and the drastic reduction in pollution levels acted as the background or baseline pollution level (Venter *et al.*, 2020; Bao and Zhang, 2020; Collivignarelli *et al.*, 2020; Dantas *et al.*, 2020; Dutheil *et al.*, 2020; Wang *et al.*, 2020; Jephcote *et al.*, 2021). Pollutants like particulate matter (PM), carbon monoxide, nitrogen dioxide, sulfur dioxide, and other trace gases showed a significant decrease in the lockdown periods (Dhaka *et al.*, 2020; Sharma *et al.*, 2020; Jain and Sharma, 2020; Mahato *et al.*, 2020). However, some species like ozone increased after lockdown restrictions were imposed, and the occurrence of several haze events was observed in the North China Plain (NCP) despite the inactivity of most of the anthropogenic primary pollutant sources (Huang *et al.*, 2020). These variabilities were attributed to the stagnant meteorological conditions and enhanced oxidative capacity in the atmosphere. But, these phenomena raise the fundamental question, what is the role of anthropogenic sources on air quality? To date, very few studies have focused on the variability in the ultrafine particle compositions over the Indian region during the lockdown period (Dave *et al.*, 2021).

Aerosols consist of a wide range of chemical species, and organic compounds are found to be the dominating fraction of the submicron aerosols (Zhang *et al.*, 2007). Organic aerosols (OA) are generally classified into primary organic aerosols (POA) and secondary organic aerosols (SOA). POA fraction refers to the aerosols directly emitted, and SOA is formed in the atmosphere via homogeneous, heterogeneous chemistry and other complex processes like photo-oxidation, nucleation, aqueous-phase reactions, and gas-to-particle partitioning of precursor gases (Kanakidou *et al.*, 2005; Ervens *et al.*, 2011; Hallquist *et al.*, 2009). The knowledge of particle composition, size distributions, temporal variations, and the contribution of different source factors are needed to understand the fine particle chemistry in different environments.

In this study, real-time measurements of the chemical constituents of non-refractory particulate matter with ≤ 1 μm aerodynamic diameter (NR-PM_1) were conducted during the pre-lockdown and lockdown periods using High-Resolution Time-of-Flight Aerosol Mass Spectrometer (HR-ToF-AMS). The temporal variation and mass size distribution of the aerosol species could give insight into the source sectors and the pollution level assuming lockdown period concentration as the baseline. The stoichiometric neutralization analysis has also been done to investigate the acidic nature of the submicron aerosols. The unit mass resolution (UMR), and high-resolution (HR) positive matrix factorization (PMF) techniques were employed to resolve the measured organic spectra into characteristic source profiles and evaluate their contribution. Back trajectories, cluster analysis, and potential source contribution function (PSCF) were also performed to investigate the potential source regions of NR-PM_1. The salient features of the size-resolved compositional analysis of submicron aerosol (NR-PM_1) with HR-ToF-AMS during the lockdown periods are presented in this manuscript.

2 DATA AND METHODOLOGY

2.1 Measurement Site

The measurements were conducted at the Indian Institute of Tropical Meteorology (IITM, 18.54°N, 73.81°E, 560 m asl), Pune as shown in Fig. S1. Pune is situated on the lee-side of the Western Ghats and is about 100 km east of the Arabian Sea. The site is surrounded by hillocks of variable heights (up to 200 m), forming a valley-like appearance. In the last few years, Pune has been experiencing tremendous growth in terms of urbanization and vehicular activity. The HR-ToF-AMS (Aerodyne Research, Inc., USA) was installed on the second floor of the institute's building at about 10 meters above the ground. The inlet was installed on the rooftop at about 12 meters above the ground. The measurement was conducted from 10 March to 17 May 2020, and a comprehensive description of the observational site and its meteorological conditions has been mentioned elsewhere (Ali *et al.*, 2012, 2016; Safai *et al.*, 2014).

2.2 High-Resolution Time-of-Flight Aerosol Mass Spectrometer (HR-ToF-AMS)

There are various methodologies like ion chromatography (IC), particle into liquid sampler

ORIGINAL RESEARCH
https://doi.org/10.4209/aaqr.220108

(PILS), Monitor for AeRosols and Gases in Ambient air (MARGA), and aerosol mass spectrometry (AMS) are available to characterize the chemical constituents of aerosols (ten Brink *et al.*, 2007; Schaap *et al.*, 2011; Acharja *et al.*, 2020). AMS excels over other measurement methods due to its fast, sensitive, versatile analytical technique providing size-resolved compositional analysis of major organic and inorganic constituents in real-time time resolution with lesser positive and negative artifacts (Jayne *et al.*, 2000; Jimenez *et al.*, 2003; Allan *et al.*, 2003). The HR-ToF-AMS data were analyzed in IGOR (Wavemetrics, Inc., Lake Oswego) using the tools named SeQUential Igor data RetRiEvaL (SQUIRREL) and Peak Integration by Key Analysis (PIKA) (Alfarra *et al.*, 2004; Drewnick *et al.*, 2005). A number of calibration methods were carried out at regular intervals during the measurement period. For example, m/z calibration was performed daily to inspect the mass spectra, and single ion signal (SIS) calibration was performed every alternate day to inspect the strength in single ion signal. The velocity calibration has also been performed with ammonium nitrate of different diameters to perform the size distribution calibrations. A detailed description of the HR-ToF-AMS instrument, its operating principle, and calibration method is discussed elsewhere, and a brief description is given in the Supplementary Section (Canagaratna *et al.*, 2007; Aiken *et al.*, 2008; Ulbrich *et al.*, 2009; Salcedo *et al.*, 2010; Lanz *et al.*, 2010).

2.3 Source Apportionment Using Positive Matrix Factorization (PMF)

In order to perform the source apportionment of OA mass spectra and separate total OA into different aerosol types, the positive matrix factorization (PMF) tool is used in this study (Paatero and Tapper, 1994; Ulbrich *et al.*, 2009). PMF is a bilinear unmixing model that does not require a priori information of the source profile or their temporal contribution and has been identified as an appropriate receptor modeling technique to quantify source contributions (Ulbrich *et al.*, 2009; Canagaratna *et al.*, 2007; Aiken *et al.*, 2008; DeCarlo *et al.*, 2006). It performs deconvolution of mass spectra (MS) into the summation of products of positively constrained mass spectral profiles and their corresponding time series under the assumption that the mass spectral profiles remain constant in time.

The measured mass concentration (X_{ij}) can be defined as per the following equation (Zhang *et al.*, 2011)

$$X_{ij} = \sum_{k=1}^{p} \left(g_{ik} \cdot f_{kj} \right) + e_{ij} \tag{1}$$

where i, j, and k represent time, variable, and particular factor, respectively. X_{ij}, g_{ik}, f_{kj}, and e_{ij} are elements of the measured organic matrix, time series of factor contributions, factor profiles, and residual matrix respectively. The model uses a least square algorithm (sum of squares of model error normalized to measurement error) to iteratively minimize the fit parameter Q, which is defined as the sum of the squares of the ratio of residual (e_{ij}) to measurement uncertainties

$$Q = \sum_{i=1}^{m} \sum_{j=1}^{n} \left(\frac{e_{ij}}{\sigma_{ij}} \right)^2 \tag{2}$$

where m is the number of samples (time series), and n is the number of variables (m/z) in the matrix. PMF can result in mathematically accurate solutions through several linear combinations of the factor profile and time series, also known as rotations. Details of the PMF source apportionment technique and its application to the AMS dataset can be found in Ulbrich *et al.* (2009) and Canagratna *et al.* (2007).

3 RESULTS AND DISCUSSION

The fundamental approach to this work is to understand how the anthropogenic sources influence aerosol loading, especially during a unique experimental situation of near-complete cessation of anthropogenic activities. This study characterizes concentrations of the organic and inorganic constituents of submicron aerosol monitored using the HR-ToF-AMS during the period

ORIGINAL RESEARCH
https://doi.org/10.4209/aaqr.220108

from 10 March to 17 May 2020. The whole period under consideration includes pre-lockdown and lockdown periods and is classified into three categories based on the efficacy of the pollution sources.

The first period spread over 10–24 March 2020 is categorized as pre-lockdown (P), characterized by the regular presence of natural and anthropogenic emission sources. The second period spread over 25 March–3 May 2020 and is categorized as lockdown-I (L1), characterized by the complete shutdown of anthropogenic emission sources like construction work, industrial activity, traffic, and other commercial activities except for essential services. However, it is mentioned that data from 25 March–29 April is not available as the instrument could not be operated in the laboratory due to strict restrictions on movement. Data during L1 was available from 30 April to 03 May 2020, and this dataset reflects the non-availability of anthropogenic pollution sources. The third period of this study spread over 4–17 May 2020 and is classified as lockdown-II (L2), characterized by partial availability of pollution sources like coal and mineral production, agricultural activities, and agro-based packaging industries. The characterization of aerosols during these periods reflects the impact of anthropogenic activities on air quality.

3.1 Temporal and Diurnal Variation of Organic and Inorganic Constituents of NR-PM_1

Mass concentrations of the organic (Org), and inorganic constituents of PM_1 and $PM_{2.5}$ during the pre-lockdown and lockdown periods are shown in Table 1, and a significant reduction in PM_1 and $PM_{2.5}$ constituents was observed during the lockdown periods. The mass fractions of NR-PM_1 constituents are presented in Fig. 1, which shows that organic and SO_4^{2-} dominated the submicron particles, followed by NO_3^- and NH_4^+. Non-refractory Cl^- was present in a significantly low fraction over Pune. From the table, it can be seen that organic mass concentrations during the P, L1, and L2 periods were 10.2 ± 6.6, 4.1 ± 2.1, and 7.3 ± 3.3 μg m^{-3}, respectively. Organic mass fraction is ubiquitous in various atmospheric environments, and the presence of a high organic fraction of PM_1 is consistent with those obtained in other parts of the world (Zhang *et al.*, 2007; Jimenez *et al.*, 2003; Cash *et al.*, 2021; Petit *et al.*, 2021; Via *et al.*, 2022). The primary sources of organic aerosols (OA) include fossil fuel burning, domestic burning (cooking and heating), and uncontained burning of vegetation and agricultural waste (Kanakidou *et al.*, 2005).

Organic mass concentrations decreased by about 60% and 29% during the L1 and L2 lockdown periods, respectively, compared to the pre-lockdown period. The average concentration of NH_4^+, SO_4^{2-}, and NO_3^- also decreased by 18%, 22%, and 53% respectively, during the lockdown period L1, which could be due to an appreciable reduction in fossil fuel and biomass burning. The concentration of NH_4^+, SO_4^{2-}, and NO_3^- during L2 was nearly equal to the values observed during the pre-lockdown period. The increase in L2 was due to the gradual resumption in services and sectors like coal and mineral production, agricultural activities, and agricultural-related packaging industries that are potential sources of fine aerosols (Singh *et al.*, 2020).

Table 1. Mass concentrations (μg m^{-3}) of NR-PM_1 organic (Org) and inorganic constituents during the (a) pre-lockdown, (b) lockdown-I, and (c) lockdown-II periods over Pune, India.

Variables	Pre-lockdown (P)	Lockdown-I (L1)	Lockdown-II (L2)
PM_{10}	73.16 ± 22.23	33.30 ± 2.36	34.70 ± 4.93
$PM_{2.5}$	44.01 ± 13.20	20.81 ± 1.47	21.69 ± 3.08
NO_x	14.11 ± 3.99	7.91 ± 0.56	10.81 ± 5.66
NR-PM_1 chemical species			
Org	10.16 ± 6.55	4.05 ± 2.13	7.25 ± 3.29
SO_4^{2-}	2.94 ± 1.41	2.30 ± 1.49	3.07 ± 1.10
NO_3^-	0.85 ± 0.52	0.40 ± 0.17	0.72 ± 0.56
Cl^-	0.17 ± 0.07	0.07 ± 0.04	0.10 ± 0.11
NH_4^+	1.08 ± 0.51	0.88 ± 0.58	1.16 ± 0.45
Estimated density of organics (ρ_{org})			
ρ_{org} (g cm^{-3})	1.14	1.28	1.35

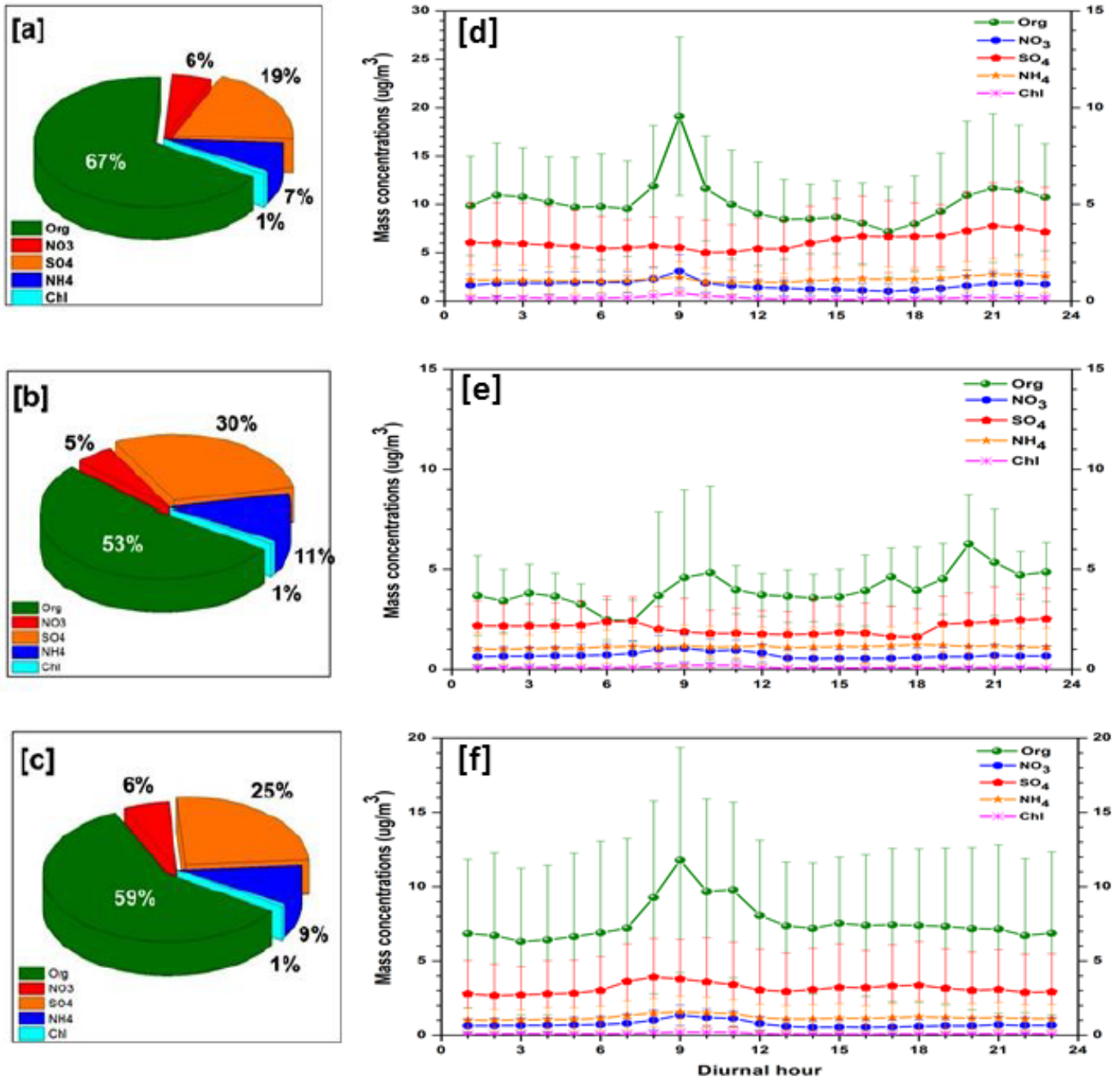

Fig. 1. Mass fractions and the diurnal variation of the Org and inorganic constituents of NR-PM_1 during the (a) pre-lockdown, (b) lockdown 1 (L1) and (c) lockdown 2 (L2) periods.

The concentration of SO_4^{2-} always remained higher than NO_3^- during the study periods. The major contribution from the thermal power plants of Mumbai (1580 MW) and Nashik (900 MW) located in the north to the northwest direction of the measurement site was the primary cause of higher sulfate than nitrate over Pune. The power sector remained operational throughout the pre-lockdown and lockdown periods and acted as the major anthropogenic pollution source sector. The nitrate concentration dropped significantly from 0.9 μg m^{-3} during pre-lockdown to 0.4 μg m^{-3} during L1. It moderately increased to 0.7 μg m^{-3} during L2, which is consistent with the temporal variation in NO_x concentrations, as shown in Table 1. The NO_3^- and NO_x concentration decrease in lockdown is mainly due to the near-complete cessation of vehicular movement in L1. The concentration of NH_4^+ was 1.1 ± 0.5, 0.9 ± 0.6, and 1.2 ± 0.5 μg m^{-3} during the P, L1, and L2 periods respectively. The variation in the concentration of NH_4^+ is not drastic as organic and nitrate due

to the unabated agro-activity of spraying fertilizer in the cultivated fields and increased soil ammonia emissions in the summertime. Non-refractory Cl^- was significantly low during the whole observational period with a minimum value of 0.1 ± 0.0 μg m^{-3} during L1 and a maximum value of 0.2 ± 0.1 μg m^{-3} during the pre-lockdown period.

Diurnal variations of the organic, SO_4^{2-}, NO_3^-, NH_4^+, and Cl^- during pre-lockdown, L1, and L2 are shown in Fig. 1. Organic showed a peak in the morning hours during the pre-lockdown period, which is a primary feature of the urban environment and mainly associated with rush hour traffic emissions and secondary productions in the atmosphere. The relatively high photochemical production in the daytime may get compensated by the loss due to the dilution effect and increased boundary layer height. The night peak in organic concentration was reduced compared to the sharp peak in the morning. During L1, the organic concentration and the sharp morning peak significantly reduced and the nighttime peak at 20:00 hrs was the highest, that could be due to the nighttime chemistry and boundary layer dynamics. During L2, organics showed a morning peak that could be due to vehicular emission as some of the vehicles were on the roads due to essential services. The diurnal cycle of the secondary inorganic aerosols (sulfate, nitrate, ammonium, and chloride) has also been investigated in Fig. 2.

The concentration in SO_4^{2-} showed short diurnal variation but is not conspicuous. The diurnal variation of nitrate showed a higher concentration during office hours in the pre-lockdown period. It reduced significantly during the lockdown periods as the vehicular emissions were significantly reduced. The diurnal variation of ammonium and chloride showed no perturbation in concentrations. The monitored secondary aerosol species are in the 1 μm size range, and the temporal variations of these species are comparatively newly explored as several studies have explored the characterization and presence of secondary species mostly in the super-micron size range of 1–2.5 μm (Sun *et al.*, 2020; Acharja *et al.*, 2022).

3.2 Size Distributions of the Constituents of NR-PM_1

The particle size distribution, chemical composition, and mass concentrations have a vital impact on the atmosphere and human health due to their size distributions (Seinfeld *et al.*, 1998; Davidson *et al.*, 2005). The HR-ToF-AMS measurements were used for the first time over Pune to assess the size-resolved compositions of aerosols in real-time. This yields information on the composition of aerosols with mass concentrations in the Aitken-mode (D_a ~10–100 nm) and the accumulation mode (Da ~100–1000 nm) (Drewnick *et al.*, 2005; DeCarlo *et al.*, 2006).

The size-resolved measurements of NR-PM_1 during the pre-lockdown and lockdown periods are shown in terms of aerosol aerodynamic diameter ($dM/d\log D_{va}$) in Fig. 2. The mass size distribution peak of fine aerosols at the smaller aerosol size ($D_{va} \leq 200$ nm) suggests the dominant presence of freshly formed aerosols over the region. A peak at a higher size range (500–600 nm) would refer to the aged and mixed regional organics particles (Zhang *et al.*, 2007). The monitored aerosols during the pre-lockdown and lockdown periods showed mass concentrations peak at the vacuum aerodynamic diameter (D_{va}) of nearly 550 nm, indicating the presence of more internally mixed, aged aerosols and less freshly emitted over Pune. The broader organic peak compared to the inorganic species illustrates the dominant nature of organic species in NR-PM_1, which is consistent with what is mentioned in Section 3.1.

3.3 Aerosol Neutralization Ratio (ANR)

The composition of atmospheric particles plays a significant role since it affects the nature of the acidity and hygroscopicity of aerosols. Direct measurements of the neutralization nature of aerosols are challenging and rare. The neutralization nature of aerosols is derived using the stoichiometric neutralization analysis. The aerosol neutralization ratio (ANR) of aerosols gives insight into the composition and characteristics of the submicron particles (Zhang *et al.*, 2007; Acharja *et al.*, 2022). The ANR is defined as follows

$$\mathrm{ANR} = \frac{\mathrm{NH_4^+\ measured\ (m)}}{\mathrm{NH_4^+\ predicted\ (p)}} \tag{3}$$

ORIGINAL RESEARCH
https://doi.org/10.4209/aaqr.220108

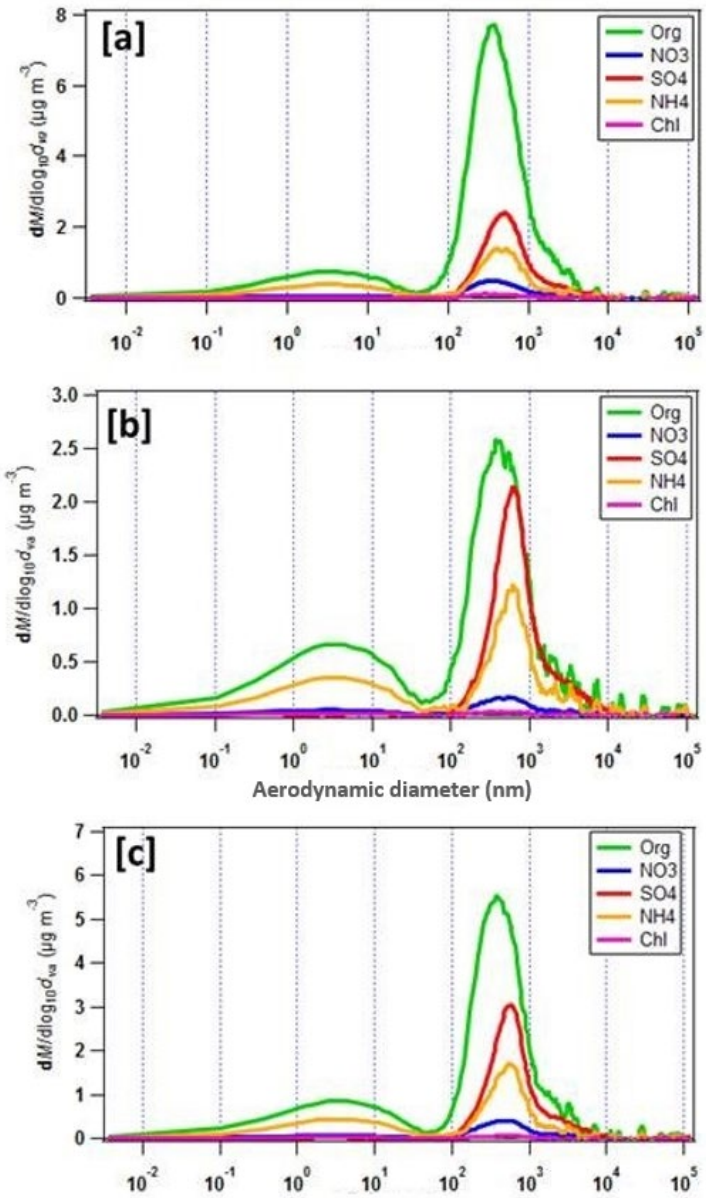

Fig. 2. The size distributions of the Org and inorganic constituents of NR-PM_1 during the (a) pre-lockdown, (b) lockdown 1 (L1) and (c) lockdown 2 (L2) periods.

$$NH_4^+(p) = \left(2 \times \frac{SO_4^{2-}(m)}{96} + \frac{NO_3^-(m)}{62} + \frac{Cl^-(m)}{35.5} \right) \quad (4)$$

where NH_4^+ (m), SO_4^{2-} (m), NO_3^- (m), and Cl^- (m) are the measured mass concentrations of ammonium, sulfate, nitrate, and chloride, respectively. The average ANR values during the pre-lockdown and lockdown periods were estimated using the aerosol composition data. During P, L1, and L2 the ANR was 0.75 ± 0.17, 0.87 ± 0.17, and 0.82 ± 0.16, respectively, showing the submicron aerosols to be mostly neutralized by ammonium during the measurement period. The presence of ammonium nitrate, ammonium sulfate, and ammonium chloride can be seen from this neutralized nature of ammonium. The ANR values showed that NH_4^+ is insufficient to neutralize all the major inorganic anionic species. The remaining fractions of the anionic species could be present in the form of organic compounds like organosulfur and organonitrate (Farmer *et al.*, 2010). However, the chemical nature, concentrations, and formation mechanisms of these compounds during the lockdown period need to be investigated in future studies.

3.4 Source Apportionment of OA Using the Unit Mass Resolution Positive Matrix Factorization (UMR-PMF)

The total measured organic species were deconvolved into the characteristic of different organic aerosol components, following the methodologies described in Ulbrich *et al.* (2009) and Zhang *et al.* (2005). Using the unit mass resolution positive matrix factorization (UMR-PMF) technique, the number of factors varied from 1 to 5 based on the diagnostic results of Q/Q_{exp} with FPeak = 0 and seed = 0. An optimal solution of four factors was chosen in this study.

The identified factors are broadly categorized as hydrocarbon-like organic aerosol (HOA) and oxygenated organic aerosol (OOA). The mass spectral distribution of HOA and OOA are physically and chemically different, and the different species in the mass spectra act as a tracer of different factors. For example, m/z 57 (mostly $C_4H_9^+$) is a tracer of HOA, m/z 44 (mostly CO_2^+) of LV-OOA, m/z 43 (mostly $C_2H_3O^+$) of SV-OOA, and m/z 60 (mostly $C_2H_4O_2^+$), and 73 (mostly $C_3H_5O_2^+$) of BBOA respectively. The mass spectra of the four-factor solution during the pre-lockdown and lockdown periods are shown in Figs. 3(a–c).

The first factor is characterized by dominant peaks at m/z = 41, 43, 55, 57, 67, 69, 71, 79, 81, 83. This spectra of aliphatic hydrocarbons (C_xH_y type ions) at m/z 41 ($C_3H_5^+$), m/z 43 ($C_3H_7^+$), m/z 55 ($C_4H_7^+$), m/z 57 ($C_4H_9^+$), m/z 67 ($C_5H_7^+$), m/z 69 ($C_5H_9^+$), m/z 71 ($C_5H_{11}^+$), m/z 79 ($C_6H_7^+$), m/z 81 ($C_6H_9^+$) and m/z 83 ($C_6H_{11}^+$) resemble HOA as reported in Zhang *et al.* (2005) and Aiken *et al.* (2008). These HOA species are a proxy of fresh vehicular and combustion emissions from diesel and gasoline engines. One of the characteristic features of HOA spectra is the higher fractional signal at m/z 43 than m/z 44. Previous studies have found a good correlation of HOA spectra with collocated measured NO_x, BC, and CO concentrations. The HOA factor averaged a quarter of OA mass over Pune.

The second factor shows significant peaks at m/z 60 ($C_2H_4O_2^+$) and 73 ($C_3H_5O_2^+$). These species correspond to the fragmentation of levoglucosan and other sugars considered as a good tracer of biomass burning emissions (Cubison *et al.*, 2011; Mohr *et al.*, 2009; Simoneit *et al.*, 1999; Hu *et al.*, 2013). The peaks at m/z 60 and 73 were insignificant in other factor profiles, implying that the factors were accurately estimated and not splitted. Biomass burning in terms of agricultural waste is not a very common phenomenon in Pune, however, cooking practices using biomasses are common in nearby residential areas. On average, this BBOA factor accounts for 15% of measured organic aerosol mass during the study period that increased from March to May as biomass burning increased in summer in the agricultural lands surrounding Pune.

The third and fourth factors represent the oxygenated organic aerosol (OOA) that generally dominates the OA fraction worldwide (Alfarra *et al.*, 2004; Lanz *et al.*, 2010). These OOA species contain aged organics that are assumed to be formed in the atmosphere from gaseous anthropogenic and biogenic precursors by photochemical and aqueous oxidation. In summer, when the temperature, solar radiation, and ozone concentration are high, affecting the volatilities variability of OOA, these OOA factors can be segregated into volatility-dependent fractions (Jimenez *et al.*, 2003; Crippa *et al.*, 2013).

One fraction shows a more prominent peak at m/z 44 and is aged, highly oxidized, and low volatile OA, whereas the other OOA is freshly oxidized, locally produced, and shows a prominent peak at m/z 43 (Ng *et al.*, 2011). The ratio of m/z 44 to m/z 43 shows the different degrees of oxidation, and the high concentrations at m/z 44 compared to m/z 43 reflect the aging process and increased degree of oxidation in the atmosphere. The ion signal at m/z 44 generally comes from the thermal decomposition of carboxylic acids and other highly oxygenated organic compounds. These species are strongly processed material and low volatile in nature, so termed as LVOOA. These species contributed the most to the OOA aerosols, contributing nearly 35% to the OA mass during the study period, similar to the inorganic SO_4^{2-} aerosols that are primarily generated from combustion sources, marine biological processes, and are long-range transported to the study location.

In contrast to this aged, highly oxidized factor, other factor shows the highest contribution at m/z 29 (CHO^+), 43 ($C_2H_3O^+$), and 55 ($C_3H_3O^+$). These oxygenated species are comparatively freshly emitted with low oxidation level suggesting a fresh, more locally produced aerosol that was quickly formed from regional precursors due to increased photochemistry during this season. These species could have originated from the nearby urban or industrial areas and started getting oxidized

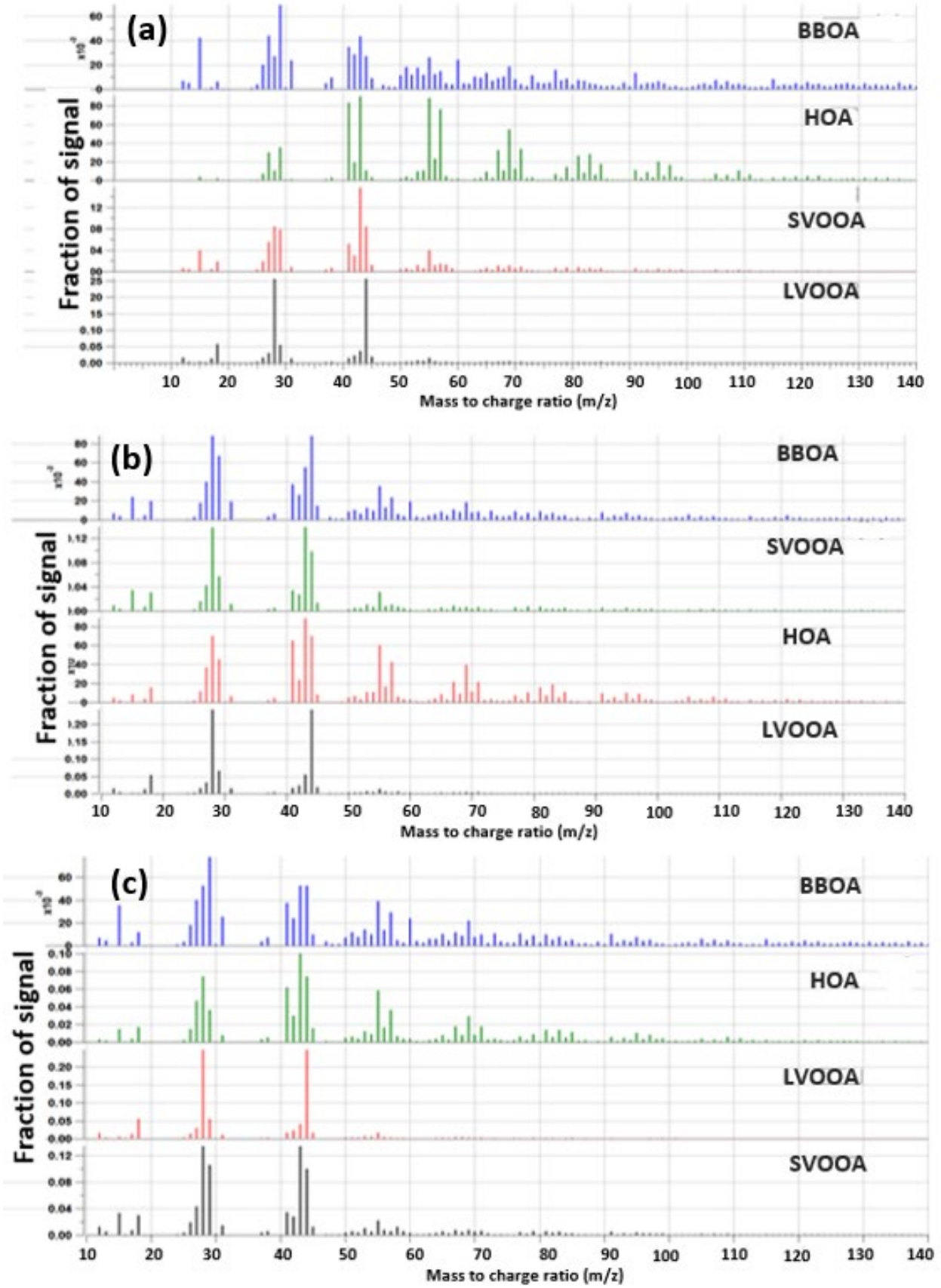

Fig. 3. Mass spectra of four factors (BBOA, HOA, SVOOA, and LVOOA) contributing to the OA components obtained from Unit Mass Resolution Positive Matrix Factorization (UMR-PMF) analysis during the (a) pre-lockdown, (b) lockdown-I, and (c) lockdown-II periods over Pune, India.

during transportation. The SVOOA contributes nearly 25% to the measured OA mass concentrations during the study period. Since HR-ToF-AMS ionizes molecules with 70 eV electron impact, the generated mass spectra for the aerosol species ensemble reflect the bulk chemical composition. On average, the primary factor contributed nearly 35–40% compared to the secondary factor contributing nearly 60–65% to the OA concentrations. Previous studies have shown that BBOA contributes less to the aerosol mass fraction compared to LVOOA and SVOOA aerosols in summer (Canagaratna *et al.*, 2015).

Freshly emitted HOA and SVOOA species contribute comparatively less, inferring the less active nature of primary emitting sources in the lockdown period. The dominating nature of secondary organic aerosol species also reveals the size distribution nature of aerosols, where more oxidized (high f44/43 ratio) aerosol generally remains in the accumulation mode.

3.5 High-Resolution Positive Matrix Factorization (HR-PMF) of Organic Aerosol (OA)

In the above section, the organic species were deconvolved into the characteristic of different organic aerosol components using the unit mass resolution (UMR) spectra. Here, we performed PMF analysis on the high-resolution (HR) AMS organic aerosol (OA) mass spectra. The factors are shown in Figs. 4(a–c), and their physical interpretability has been discussed here.

The HR-PMF analysis divides the total OA into four factors similar to UMR-PMF analyses. The elemental ratios (H/C and O/C) of organic aerosols are used, which provides crucial information for understanding the phase state and atmospheric aging of aerosols (Aiken *et al.*, 2008; Zhang *et al.*, 2011). These elemental ratios exhibited large variation during prevailing conditions, e.g., H/C varied from 1.36 to 1.93 with the highest value in the pre-lockdown period and O/C varied from 0.17 to 0.98 with the highest value in the lockdown period. The increased O/C ratio suggested that the bulk OA composition had relatively more oxygenated compounds during lockdown. The organic mass-to-carbon (OM/OC) ratio during different lockdown periods varied from 1.28 to 2.46. The slight decrease in O/C and increase in H/C during pre-lockdown to lockdown periods is likely due to emissions of primary hydrocarbon-like organic aerosols from fuel combustions which were almost non-existent during lockdown periods. The variability in O/C during the study period from other periods could be due to the impact of the aqueous phase processing of aerosols in clouds that increases the O/C of organics.

Using the elemental ratios, the density of organics (ρ_{org}) can be estimated following the methodologies of Kuwata *et al.* (2012):

$$\rho_{org} = \frac{\left[12 + 1\times\left(\frac{H}{C}\right) + 1.6\times\left(\frac{O}{C}\right)\right]}{\left[7 + 5\times\left(\frac{H}{C}\right) + 4.15\times\left(\frac{O}{C}\right)\right]} \quad (5)$$

In which ρ_{org} is expressed in g cm^{-3}, and H/C and O/C are the average values during different measurement periods of this study. We find the predicted ρ_{org} during pre-lockdown, lockdown-I, and lockdown-II periods to be 1.14, 1.28, and 1.35 respectively, to be similar to the reference value i.e., 1.30 g cm^{-3} (Chen *et al.*, 2015; Canagaratna *et al.*, 2015).

The different factors are characterized by their different elemental ratios, like hydrocarbon-loke OA (HOA) showed high H/C = 1.93 and low O/C = 0.17 value, whereas oxygenated OA (LVOOA and SVOOA) showed high O/C and low H/C ratio. A number of previous studies have also found similar properties in the elemental ratios of OA factors. The different volatility profiles of these factors follow the pattern of the worldwide datasets reported in Jimenez *et al.* (2003) and Ng *et al.* (2011). Primary organic aerosol species like HOA shows higher H/C and lower O/C values, and a higher N/C ratio is observed when higher interaction of organics with NH_3 occurs. The variability in H/C, O/C, and OM/OC ratios for HOA, LV-OOA, SV-OOA, and BBOA during the study period are shown in Fig. 4, and all these elemental ratios showed distinct characteristics during different periods.

ORIGINAL RESEARCH
https://doi.org/10.4209/aaqr.220108

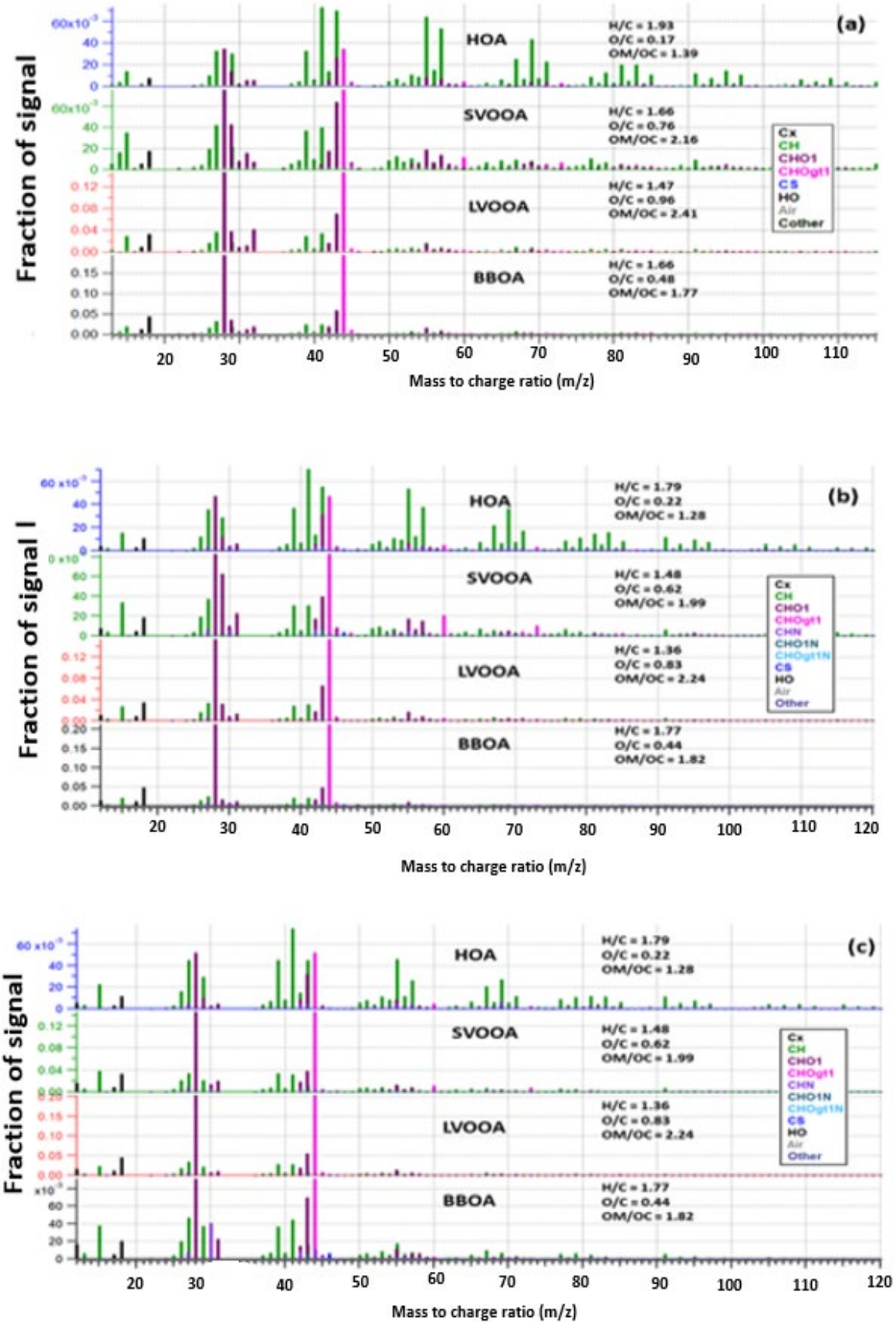

Fig. 4. High-resolution positive matrix factorization (HR-PMF) spectra of four OA factors (BBOA, HOA, SVOOA, and LVOOA) obtained during the (a) pre-lockdown, (b) lockdown-I, and (c) lockdown-II periods over Pune, India. Using the elemental ratios (H/C, O/C), the density of organics (ρ_{org}) can be estimated.

3.6 Back Trajectory and Cluster Analysis

The influence of air mass origin on the species concentrations was investigated by tracing the path of the air masses reaching the study location. During the study period, 24-hour backward trajectories were obtained using the HYSPLIT model (Stohl, 1996; Draxler and Rolph, 2003) at an altitude of 500 m above ground level (AGL) every hour for each day. This height was chosen which minimizes the effect of surface friction and represents winds in the lower boundary layer (Begum *et al.*, 2005; Gao *et al.*, 1993). The estimated back trajectories were then grouped into clusters using the trajectory endpoints (lat, long), and each cluster represents different geographical origins (Dumka *et al.*, 2013).

These clusters determine and demarcate the relative importance of regional and distant source regions. Various receptor models have been developed, combining meteorology with the measured chemical compositions to determine the preferred pathways that give rise to the observed high particle concentrations at the sampling site (Hopke, 2003). The primary criterion of trajectory clustering is to minimize the variability among the trajectories within a cluster and maximize the variability between the clusters (Vinoj *et al.*, 2010). The optimal number of clusters was assessed from the variation of total spatial variance (TSV), and when TSV increased rapidly, that cluster number has been used in the analysis (Draxler, 1992).

In our analysis, 3 clusters were identified as the final simulated cluster trajectories. The back trajectory and cluster analysis of the measurement period are shown in Fig. 5. Based on the trajectory analysis, the most common wind directions contributing to PM concentrations were from the west and northwest directions, carrying air masses primarily from land and ocean. Cluster analysis revealed three major clusters representing the mean trajectory pathways. In the pre-lockdown period, the majority of air parcels were coming from two regions, the north, and northwest directions. While during the lockdown period, air masses were predominantly from the northwest. These air mass trajectories are consistent with the previous studies reported by Ali *et al.* (2012) over the same study location. Cluster 1 was the major cluster representing 57% of air masses that might have traveled through Mumbai to reach Pune, which carried more pollutants to Pune. Cluster 2 represented 27.8% of air masses from the northwest direction, primarily originating from the coastal regions, the Arabian Sea, and to some extent from Gujarat and the Thar Desert. Cluster 3 represented 14.4% of regional air masses near Pune, depicting major source regions near neighboring areas. The mass concentrations of the different NR-PM_1 components and the air mass direction combinations might give an insight into the geographical origins of chemical species.

3.7 Weighted Potential Source Contribution Function (WPSCF)

Fig. 6 shows the PSCF results in the form of maps of the measurement location on which the weighted PSCF (WPSCF) values ranging from 0 to 1 are displayed in terms of a color scale. For PSCF analysis, the domain covered by the trajectories was divided into grids with $0.2° \times 0.2°$ resolutions. These cells are indicative of areas of potential contributions for PM pollutants, and grid cells with higher PSCF values are more likely to contribute to the constituent pollutants. The spatial distribution of WPSCF values shows that WPSCF > 0.7 was over the north and northwest parts of Pune, indicating these locations to be the major source areas of PM. From the distribution of WPSCF values, it can be seen that the sources most likely to affect Pune are located in the (1) industrialized and populated city of Mumbai, indicating shorter transport pathways (2) the coastal and ocean region of the Arabian Sea (3) industrial regions of Rajasthan and Gujarat region.

The PSCF plots highlight the dominant oceanic origin of the constituents of NR-PM_1, and some chemical species are transported or formed above the ocean rather than directly emitted by sea spray (Ovadnevaite *et al.*, 2012). Under the influence of air masses from the Arabian Sea, emissions of dimethyl sulfide (DMS) and organosulfur compounds by microorganisms could contribute to the observed Org and SO_4 concentrations (Luria *et al.*, 1996). Previous studies have also shown the contribution of sulfur and Org matter from the marine air in PM_1 chemical compositions (Fomba *et al.*, 2014). These species may also be released by maritime traffic across coastal regions, shipping emissions, and anthropogenic activities in distant continental parts, whose emissions may be carried toward the ocean and brought back to Pune by western winds. During the transport of Org over the ocean surface, SOA formation also enhances, which under specific atmospheric conditions can be initiated by chlorine atoms (Hallquist *et al.*, 2009; Hossaini *et al.*, 2016).

ORIGINAL RESEARCH
https://doi.org/10.4209/aaqr.220108

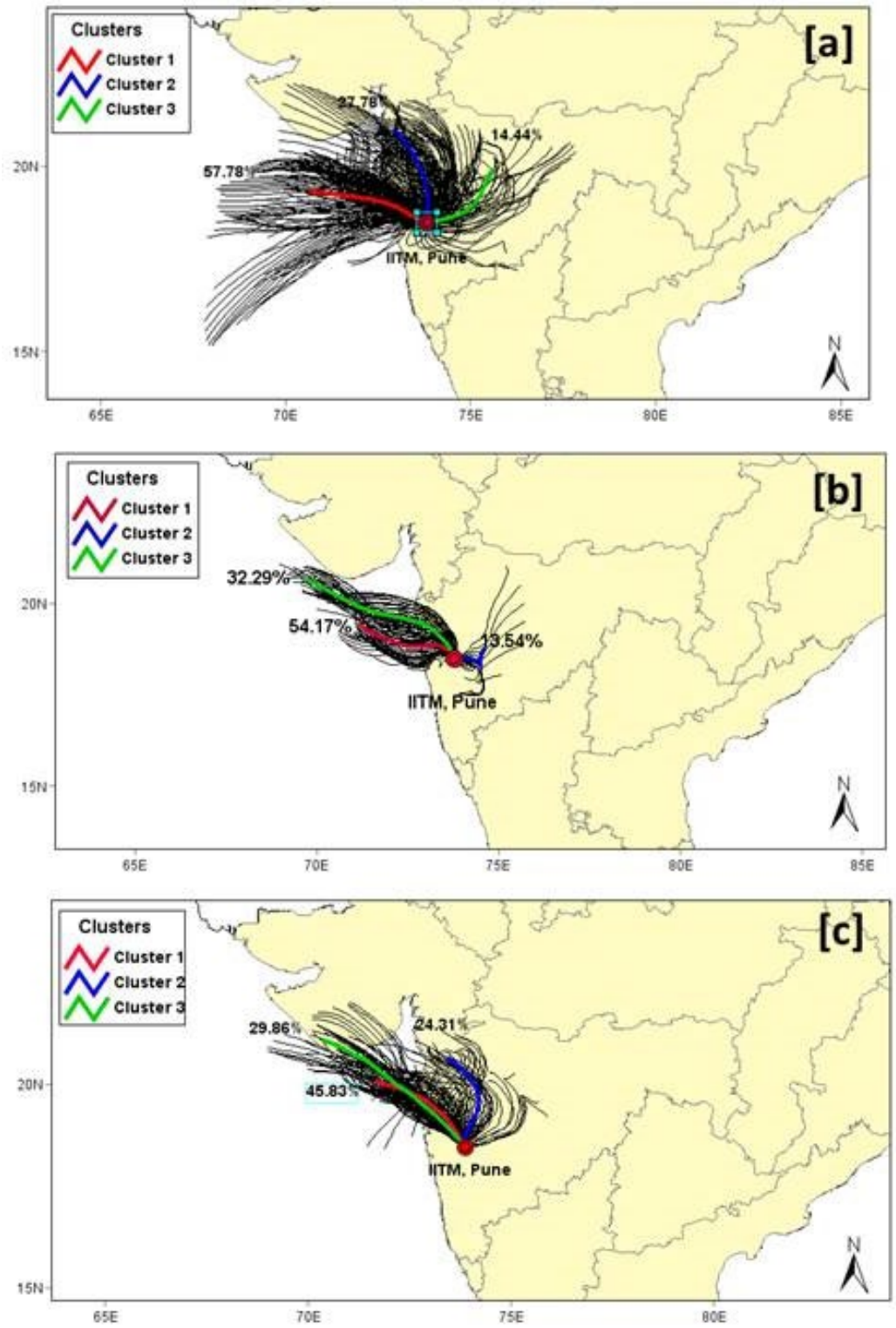

Fig. 5. The 24 h backward trajectories of air masses at 500 m above ground level arriving at the measurement location. All the near trajectories were merged to a mean trajectory to represent the entire groups by cluster analysis.

Sources located in Mumbai may influence PM by direct emissions through industrial activities, biomass and waste burning, dense populations, and high traffic emissions under prevailing meteorological conditions. Recirculating narrow and short trajectories from these adjoining regions result in high source contributions at the receptor site. PSCF maps showed a high frequency of

ORIGINAL RESEARCH
https://doi.org/10.4209/aaqr.220108

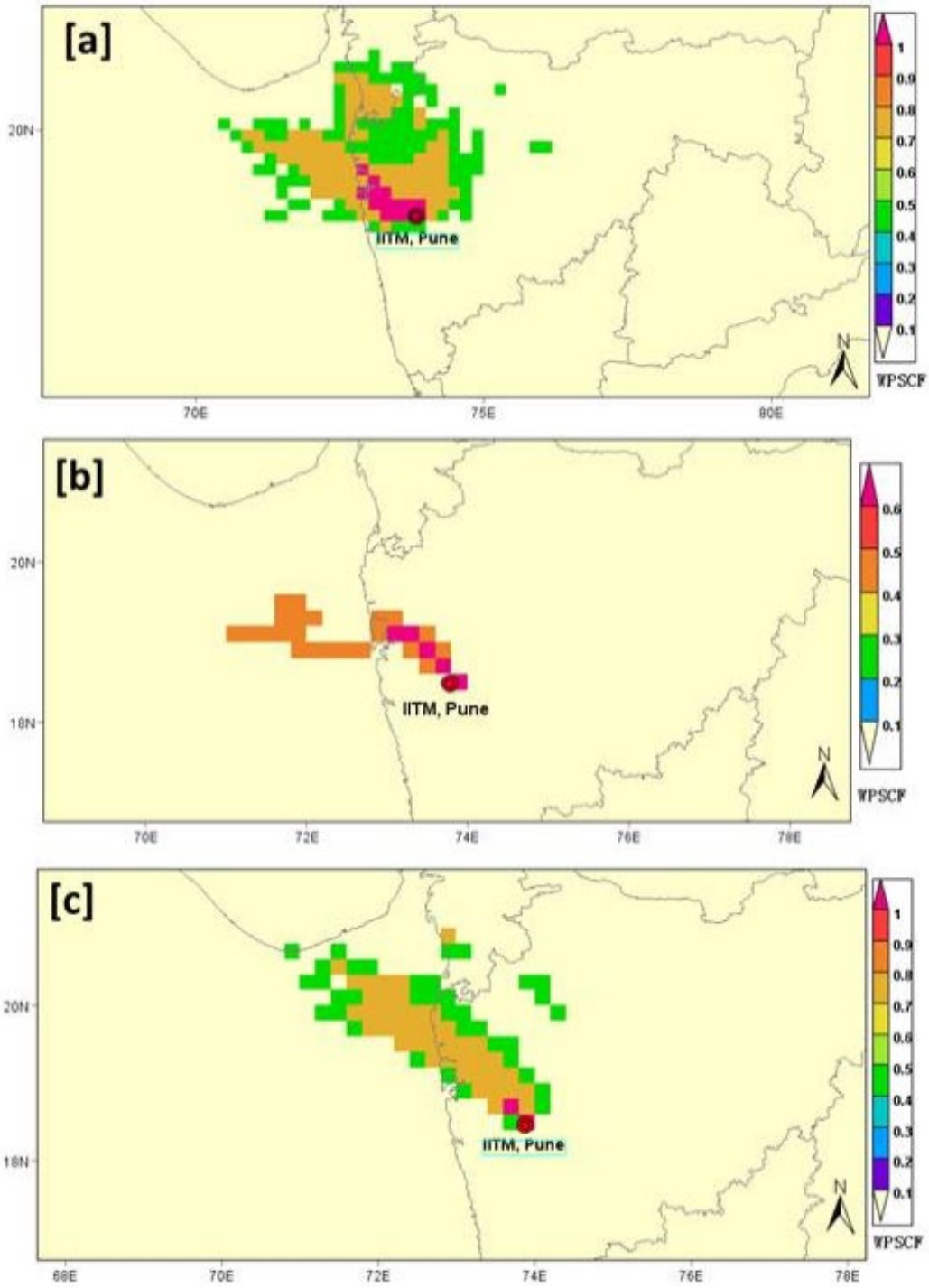

Fig. 6. Potential source contribution function (PSCF) plots of NR-PM_1 during the (a) pre-lockdown, (b) lockdown 1 (L1) and (c) lockdown 2 (L2) periods.

potential source location (WPSCF > 0.7) over industrialized areas of Maharashtra. Air masses from the southern part of the measurement location impact less to the pollutant concentrations.

The northern source regions are responsible for bringing significant dust in the summer season from regions like Rajasthan. Sources in the nearby regions also appear to be important sources for PM especially due to regional sources like biomass burning, waste burning, brick kilns, construction activities, and thermal power plants. Thus, from the assessment of clusters and spatial variation of WPSCF, the potential source sectors can be estimated, helping in policymaking to control emissions.

ORIGINAL RESEARCH
https://doi.org/10.4209/aaqr.220108

4 SUMMARY AND CONCLUSIONS

In this study, we present the comprehensive temporal variation and physicochemical characterization of Org and inorganic constituents of NR-PM_1 measured with an HR-ToF-AMS instrument during the pre-lockdown and lockdown periods in India. This kind of real-time high temporal resolution measurement of submicron particles is particularly relevant in India, where air pollution affects the population to a great extent. This assessment would characterize the submicron aerosol (NR-PM_1) possibly impacted by different source regions during the COVID-19 lockdown restrictions. The following conclusions can be made from this study:

The composition data of NR-PM_1 over Pune showed that Org dominated the mass fractions of submicron aerosols with nearly 60% contribution. The mass concentration was followed by sulfate, ammonium, and nitrate. Non-refractory chloride contributed very little to the PM_1 mass fractions.

During the lockdown period, the Org and nitrate concentrations decreased by 60% and 53% from the pre-lockdown period. The significant reduction in the primary emission from traffic, coal combustion, and regional biomass burning might have impacted the reduction in concentrations.

The size-resolved submicron aerosol measurements showed the peaks of Org and inorganic constituents at an aerodynamic diameter of 550 nm, referring to the higher presence of aged, oxidized constituents and less freshly emitted aerosols in Pune. These peaks could also be due to the regional secondary aerosol formation from the gaseous precursors and strong oxidation in the urban environment.

Unit mass resolution positive matrix factorization (UMR-PMF) analysis was applied to the OA mass spectra and four OA factors were identified, hydrogenated organic aerosol (HOA), biomass burning organic aerosol (BBOA), low volatile oxygenated organic aerosol (LVOOA), and semi-volatile oxygenated organic aerosol (SVOOA).

The oxygenated organic aerosol (OOA) contributed more (60%) to the OA mass compared to hydrogenated organic aerosol (HOA) (40%). Among the OA factors, LVOOA contributed the most, similar to the inorganic SO_4^{2-} species. The HOA factor corresponded primarily to vehicular emission, whereas the BBOA factor corresponds to biomass burning. The two OOA species LVOOA and SVOOA correspond to the secondary formation mainly from the photochemical and aqueous phase oxidation of the precursors.

The diurnal variations of the constituents showed the dominant role of vehicular emission and boundary layer dynamics affecting the ambient concentrations. High emissions from vehicles mostly contributed to the nitrate concentration and led to the two concentration peaks in nitrate during office hours in the morning and evening. Whereas during the lockdown period, the concentrations showed almost constant values at all hours with no peaks or perturbation in the diurnal signal.

Back trajectories, cluster analysis, and PSCF analysis identified Mumbai and the Arabian Sea as potential source regions of air masses and responsible for the regional aerosol loading during the observation period.

High-Resolution Positive Matrix factorization (HR-PMF) analysis divides the total OA into four factors, similar to UMR analyses. The elemental ratios (H/C and O/C) of organic aerosols are used, which provides crucial information to understand the phase state and ageing of aerosols. These elemental ratios exhibited large variation during prevailing conditions, e.g., H/C varied between 1.36 to 1.93 with the highest value in the pre-lockdown period and O/C varied between 0.17 to 0.98 with the highest value in the lockdown period. The increased O/C ratio suggested that the bulk OA composition had relatively more oxygenated compounds during lockdown.

Using these ratios, we estimated the ρ_{org} during pre-lockdown, lockdown-I, and lockdown-II periods to be 1.14, 1.28, and 1.35 g cm^{-3} respectively. The stoichiometric neutralization analysis showed the aerosol neutralization ratio (ANR) to be nearly 0.8, implying the higher presence of ammonium salts like ammonium sulfate and ammonium nitrate over Pune.

ADDITIONAL INFORMATION AND DECLARATIONS

Data Availability

All the data used to prepare the manuscript are archived on the Prithvi (IITM) super-computer and can be provided upon request to the corresponding authors.

Author Contributions

All authors contributed to the research; PA and SDG designed the research; PA conducted the research and wrote the paper; AV, KA, and SDG contributed to the writing; AV, PL, SWG, SD, NGD, KA, GG, and SDG formulated the research.

Competing Interests

The authors declare that they have no conflict of interest

Acknowledgments

We thank the Director of the Indian Institute of Tropical Meteorology (IITM), for his continuous support and encouragement. IITM is funded by the Ministry of Earth Sciences (MoES), the Government of India. The data used to prepare the manuscript is available in the IITM cloud storage and can be provided upon request to the corresponding author. The fellowship of P.A. and A.V. was supported by the National Supercomputing Mission (NSM) program grant at C-DAC, and we are grateful to the Executive Director and the Director-General of C-DAC.

Supplementary Material

Supplementary material for this article can be found in the online version at https://doi.org/10.4209/aaqr.220108

REFERENCES

Aan de Brugh, J.M.J., Henzing, J.S., Schaap, M., Morgan, W.T., van Heerwaarden, C.C., Weijers, E.P., Coe, H., Krol, M.C. (2012). Modelling the partitioning of ammonium nitrate in the convective boundary layer. Atmos. Chem. Phys. 12, 3005–3023. https://doi.org/10.5194/acp-12-3005-2012

Acharja, P., Ali, K., Trivedi, D.K., Safai, P.D., Ghude, S., Prabhakaran, T., Rajeevan, M. (2020). Characterization of atmospheric trace gases and water soluble inorganic chemical ions of PM_1 and $PM_{2.5}$ at Indira Gandhi International Airport, New Delhi during 2017–18 winter. Sci. Total Environ. 729, 138800. https://doi.org/10.1016/j.scitotenv.2020.138800

Acharja, P., Ali, K., Ghude, S.D., Sinha, V., Sinha, B., Kulkarni, R., Gultepe, I., Rajeevan, M.N. (2022). Enhanced secondary aerosol formation driven by excess ammonia during fog episodes in Delhi, India. Chemosphere, 289, 133155. https://doi.org/10.1016/j.chemosphere.2021.133155

Agarwal, A., Kaushik, A., Kumar, S., Mishra, R.K. (2020). Comparative study on air quality status in Indian and Chinese cities before and during the COVID-19 lockdown period. Air Qual. Atmos. Health 13, 1167–1178. https://doi.org/10.1007/s11869-020-00881-z

Aiken, A.C., Decarlo, P.F., Kroll, J.H., Worsnop, D.R., Huffman, J.A., Docherty, K.S., Ulbrich, I.M., Mohr, C., Kimmel, J.R., Sueper, D., Sun, Y. (2008). O/C and OM/OC ratios of primary, secondary, and ambient organic aerosols with high-resolution time-of-flight aerosol mass spectrometry. Environ. Sci. Technol. 42, 4478–4485. https://doi.org/10.1021/es703009q

Alfarra, M.R., Coe, H., Allan, J.D., Bower, K.N., Boudries, H., Canagaratna, M.R., Jimenez, J.L., Jayne, J.T., Garforth, A.A., Li, S.M., Worsnop, D.R. (2004). Characterization of urban and rural organic particulate in the lower Fraser valley using two aerodyne aerosol mass spectrometers. Atmos. Environ. 38, 5745–5758. https://doi.org/10.1016/j.atmosenv.2004.01.054

Ali, K., Budhavant, K.B., Safai, P.D., Rao, P.S.P. (2012). Seasonal factors influencing in chemical composition of total suspended particles at Pune, India. Sci. Total Environ. 414, 257–267. https://doi.org/10.1016/j.scitotenv.2011.09.011

Ali, K., Panicker, A.S., Beig, G., Srinivas, R., Acharja, P. (2016). Carbonaceous aerosols over Pune and Hyderabad (India) and influence of meteorological factors. J. Atmos. Chem. 73, 1–27. https://doi.org/10.1007/s10874-015-9314-4

Allan, J.D., Jimenez, J.L., Williams, P.I., Alfarra, M.R., Bower, K.N., Jayne, J.T., Coe, H., Worsnop, D.R. (2003). Quantitative sampling using an Aerodyne aerosol mass spectrometer 1. Techniques of data interpretation and error analysis. J. Geophys. Res. 108, 4090. https://doi.org/10.1029/2002JD002358

Bao, R., Zhang, A. (2020). Does lockdown reduce air pollution? Evidence from 44 cities in northern

China. Sci. Total Environ. 731, 139052. https://doi.org/10.1016/j.scitotenv.2020.139052

Begum, B.A., Kim, E., Jeong, C.H., Lee, D.W., Hopke, P.K. (2005). Evaluation of the potential source contribution function using the 2002 Quebec forest fire episode. Atmos. Environ. 39, 3719–3724. https://doi.org/10.1016/j.atmosenv.2005.03.008

Canagaratna, M.R., Jayne, J.T., Jimenez, J.L., Allan, J.D., Alfarra, M.R., Zhang, Q., Onasch, T.B., Drewnick, F., Coe, H., Middlebrook, A., Delia, A. (2007). Chemical and microphysical characterization of ambient aerosols with the aerodyne aerosol mass spectrometer. Mass Spectrom. Rev. 26, 185–222. https://doi.org/10.1002/mas.20115

Canagaratna, M.R., Jimenez, J.L., Kroll, J.H., Chen, Q., Kessler, S.H., Massoli, P., Hildebrandt Ruiz, L., Fortner, E., Williams, L.R., Wilson, K.R., Surratt, J.D. (2015). Elemental ratio measurements of organic compounds using aerosol mass spectrometry: Characterization, improved calibration, and implications. Atmos. Chem. Phys. 15, 253–272. https://doi.org/10.5194/acp-15-253-2015

Cash, J.M., Langford, B., Di Marco, C., Mullinger, N.J., Allan, J., Reyes-Villegas, E., Joshi, R., Heal, M.R., Acton, W.J.F., Hewitt, C.N., Misztal, P.K. (2021). Seasonal analysis of submicron aerosol in Old Delhi using high-resolution aerosol mass spectrometry: chemical characterisation, source apportionment and new marker identification. Atmos. Chem. Phys. 21, 10133–10158. https://doi.org/10.5194/acp-21-10133-2021

Chen, Q., Heald, C.L., Jimenez, J.L., Canagaratna, M.R., Zhang, Q., He, L.Y., Huang, X.F., Campuzano-Jost, P., Palm, B.B., Poulain, L., Kuwata, M. (2015). Elemental composition of organic aerosol: The gap between ambient and laboratory measurements. Geophys. Res. Lett. 42, 4182–4189. https://doi.org/10.1002/2015GL063693

Collivignarelli, M.C., Abbà, A., Bertanza, G., Pedrazzani, R., Ricciardi, P. and Miino, M.C., 2020. Lockdown for CoViD-2019 in Milan: What are the effects on air quality? Sci. Total Environ. 732, 139280. https://doi.org/10.1016/j.scitotenv.2020.139280

Crippa, M., DeCarlo, P.F., Slowik, J.G., Mohr, C., Heringa, M.F., Chirico, R., Poulain, L., Freutel, F., Sciare, J., Cozic, J. and Di Marco, C.F., 2013. Wintertime aerosol chemical composition and source apportionment of the organic fraction in the metropolitan area of Paris. Atmos. Chem. Phys. 13, 961–981. https://doi.org/10.5194/acp-13-961-2013

Cubison, M.J., Ortega, A.M., Hayes, P.L., Farmer, D.K., Day, D., Lechner, M.J., Brune, W.H., Apel, E., Diskin, G.S., Fisher, J.A., Fuelberg, H.E. (2011). Effects of aging on organic aerosol from open biomass burning smoke in aircraft and laboratory studies. Atmos. Chem. Phys. 11, 12049–12064. https://doi.org/10.5194/acp-11-12049-2011

Dantas, G., Siciliano, B., França, B.B., da Silva, C.M., Arbilla, G. (2020). The impact of COVID-19 partial lockdown on the air quality of the city of Rio de Janeiro, Brazil. Sci. Total Environ. 729, 139085. https://doi.org/10.1016/j.scitotenv.2020.139085

Dave, J., Meena, R., Singh, A., Rastogi, N. (2021). Effect of COVID-19 lockdown on the concentration and composition of NR-$PM_{2.5}$ over Ahmedabad, a big city in western India. Urban Clim. 37, 100818. https://doi.org/10.1016/j.uclim.2021.100818

Davidson, C.I., Phalen, R.F., Solomon, P.A. (2005). Airborne particulate matter and human health: A review. Aerosol Sci. Technol. 39, 737–749. https://doi.org/10.1080/02786820500191348

DeCarlo, P.F., Kimmel, J.R., Trimborn, A., Northway, M.J., Jayne, J.T., Aiken, A.C., Gonin, M., Fuhrer, K., Horvath, T., Docherty, K.S., Worsnop, D.R. (2006). Field-deployable, high-resolution, time-of-flight aerosol mass spectrometer. Anal. Chem. 78, 8281–8289. https://doi.org/10.1021/ac061249n

Dhaka, S.K., Kumar, V., Panwar, V., Dimri, A.P., Singh, N., Patra, P.K., Matsumi, Y., Takigawa, M., Nakayama, T., Yamaji, K., Kajino, M. (2020). $PM_{2.5}$ diminution and haze events over Delhi during the COVID-19 lockdown period: an interplay between the baseline pollution and meteorology. Sci. Rep. 10, 1–8. https://doi.org/10.1038/s41598-020-70179-8

Draxler, R.R. (1992). Hybrid single-particle Lagrangian integrated trajectories (HY-SPLIT), Version 3.0: User's guide and model description (p. 26). US Department of Commerce, National Oceanic and Atmospheric Administration, Environmental Research Laboratories, Air Resources Laboratory. www.arl.noaa.gov/documents/reports/ARL%20TM-195.pdf

Draxler, R.R., Rolph, G.D. (2003). HYSPLIT (HYbrid Single-particle Lagrangian Integrated Trajectory). NOAA Air Resources Laboratory, Silver Spring, MD Model access via NOAA ARL READY Website. http://www.arl.noaa.gov/ready/hysplit4.html

Drewnick, F., Hings, S.S., DeCarlo, P., Jayne, J.T., Gonin, M., Fuhrer, K., Weimer, S., Jimenez, J.L.,

Demerjian, K.L., Borrmann, S., Worsnop, D.R. (2005). A new time-of-flight aerosol mass spectrometer (TOF-AMS)—Instrument description and first field deployment. Aerosol Sci. Technol. 39, 637–658. https://doi.org/10.1080/02786820500182040

Dumka, UC, Manchanda, R.K., Sinha, P.R., Sreenivasan, S., Moorthy, K.K., Babu, S.S. (2013). Temporal variability and radiative impact of black carbon aerosol over tropical urban station Hyderabad. J. Atmos. Sol. Terr. Phys. 105, 81–90. https://doi.org/10.1016/j.jastp.2013.08.003

Dutheil, F., Baker, J.S., Navel, V. (2020). COVID-19 as a factor influencing air pollution? Environ. Pollut. 263, 114466. https://doi.org/10.1016/j.envpol.2020.114466

Ervens, B., Turpin, B.J., Weber, R.J. (2011). Secondary organic aerosol formation in cloud droplets and aqueous particles (aqSOA): A review of laboratory, field and model studies. Atmos. Chem. Phys. 11, 11069–11102. https://doi.org/10.5194/acp-11-11069-2011

Farmer, D.K., Matsunaga, A., Docherty, K.S., Surratt, J.D., Seinfeld, J.H., Ziemann, P.J., Jimenez, J.L. (2010). Response of an aerosol mass spectrometer to organonitrates and organosulfates and implications for atmospheric chemistry. PNAS 107, 6670–6675. https://doi.org/10.1073/pnas.0912340107

Fomba, K.W., Müller, K., van Pinxteren, D., Poulain, L., van Pinxteren, M., Herrmann, H. (2014). Long-term chemical characterization of tropical and marine aerosols at the Cape Verde Atmospheric Observatory (CVAO) from 2007 to 2011. Atmos. Chem. Phys. 14, 8883–8904. https://doi.org/10.5194/acp-14-8883-2014

Gao, N., Cheng, M.D., Hopke, P.K. (1993). Potential source contribution function analysis and source apportionment of sulfur species measured at Rubidoux, CA during the southern California air quality study, 1987. Anal. Chim. Acta 277, 369–380. https://doi.org/10.1016/0003-2670(93)80449-U

Hallquist, M., Wenger, J.C., Baltensperger, U., Rudich, Y., Simpson, D., Claeys, M., Dommen, J., Donahue, N.M., George, C., Goldstein, A.H., Hamilton, J.F. (2009). The formation, properties and impact of secondary organic aerosol: Current and emerging issues. Atmos. Chem. Phys. 9, 5155–5236. https://doi.org/10.5194/acp-9-5155-2009

Hopke, P.K. (2003). Recent developments in receptor modeling. J. Chemom. 17, 255–265. https://doi.org/10.1002/cem.796

Hossaini, R., Chipperfield, M.P., Saiz-Lopez, A., Fernandez, R., Monks, S., Feng, W., Brauer, P., Von Glasow, R. (2016). A global model of tropospheric chlorine chemistry: Organic versus inorganic sources and impact on methane oxidation. J. Geophys. Res. 121, 14271–14297. https://doi.org/10.1002/2016JD025756

Hu, Q.H., Xie, Z.Q., Wang, X.M., Kang, H., Zhang, P. (2013). Levoglucosan indicates high levels of biomass burning aerosols over oceans from the Arctic to Antarctic. Sci. Rep. 3, 1–7. https://doi.org/10.1038/srep03119

Huang, X., Ding, A., Gao, J., Zheng, B., Zhou, D., Qi, X., Tang, R., Wang, J., Ren, C., Nie, W., Chi, X., Xu, Z., Chen, L., Li, Y., Che, F., Pang, N., Wang, H., Tong, D., Qin, W., Cheng, W., *et al.* (2021). Enhanced secondary pollution offset reduction of primary emissions during COVID-19 lockdown in China. Natl. Sci. Rev. 8, nwaa137. https://doi.org/10.1093/nsr/nwaa137

Jain, S., Sharma, T. (2020). Social and travel lockdown impact considering coronavirus disease (COVID-19) on air quality in megacities of India: Present benefits, future challenges and way forward. Aerosol Air Qual. Res. 20, 1222–1236. https://doi.org/10.4209/aaqr.2020.04.0171

Jayne, J.T., Leard, D.C., Zhang, X., Davidovits, P., Smith, K.A., Kolb, C.E., Worsnop, D.R. (2000). Development of an aerosol mass spectrometer for size and composition analysis of submicron particles. Aerosol Sci. Technol. 33, 49–70. https://doi.org/10.1080/027868200410840

Jephcote, C., Hansell, A.L., Adams, K., Gulliver, J. (2021). Changes in air quality during COVID-19' lockdown'in the United Kingdom. Environ. Pollut. 272, 116011. https://doi.org/10.1016/j.envpol.2020.116011

Jimenez, J.L., Jayne, J.T., Shi, Q., Kolb, C.E., Worsnop, D.R., Yourshaw, I., Seinfeld, J.H., Flagan, R.C., Zhang, X., Smith, K.A., Morris, J.W. (2003). Ambient aerosol sampling using the aerodyne aerosol mass spectrometer. J. Geophys. Res. 108, 8425. https://doi.org/10.1029/2001JD001213

Kanakidou, M., Seinfeld, J.H., Pandis, S.N., Barnes, I., Dentener, F.J., Facchini, M.C., Van Dingenen, R., Ervens, B., Nenes, A., Nielsen, C.J., Swietlicki, E., Putaud, J.P., Balkanski, Y., Fuzzi, S., Horth, J., Moortgat, G.K., Winterhalter, R., Myhre, C.E.L., Tsigaridis, K., Vignati, E., *et al.* (2005).

Organic aerosol and global climate modelling: A review. Atmos. Chem. Phys. 5, 1053–1123. https://doi.org/10.5194/acp-5-1053-2005

Kuwata, M., Zorn, S.R., Martin, S.T. (2012). Using elemental ratios to predict the density of organic material composed of carbon, hydrogen, and oxygen. Environ. Sci. Technol. 46, 787–794. https://doi.org/10.1021/es202525q

Lanz, V.A., Prévôt, A.S.H., Alfarra, M.R., Weimer, S., Mohr, C., DeCarlo, P.F., Gianini, M.F.D., Hueglin, C., Schneider, J., Favez, O., d'Anna, B. (2010). Characterization of aerosol chemical composition with aerosol mass spectrometry in Central Europe: an overview. Atmos. Chem. Phys. 10, 10453. https://doi.org/10.5194/acp-10-10453-2010

Luria, M., Peleg, M., Sharf, G., Tov-Alper, D.S., Spitz, N., Ben Ami, Y., Gawii, Z., Lifschitz, B., Yitzchaki, A., Seter, I. (1996). Atmospheric sulfur over the east Mediterranean region. J. Geophys. Res. 101, 25917–25930. https://doi.org/10.1029/96JD01579

Mahato, S., Pal, S., Ghosh, K.G. (2020). Effect of lockdown amid COVID-19 pandemic on air quality of the megacity Delhi, India. Sci. Total Environ. 730, 139086. https://doi.org/10.1016/j.scitotenv.2020.139086

Mohr, C., Huffman, J.A., Cubison, M.J., Aiken, A.C., Docherty, K.S., Kimmel, J.R., Ulbrich, I.M., Hannigan, M., Jimenez, J.L. (2009). Characterization of primary organic aerosol emissions from meat cooking, trash burning, and motor vehicles with high-resolution aerosol mass spectrometry and comparison with ambient and chamber observations. Environ. Sci. Technol. 43, 2443–2449. https://doi.org/10.1021/es8011518

Ng, N.L., Herndon, S.C., Trimborn, A., Canagaratna, M.R., Croteau, P.L., Onasch, T.B., Sueper, D., Worsnop, D.R., Zhang, Q., Sun, Y.L., Jayne, J.T. (2011). An Aerosol Chemical Speciation Monitor (ACSM) for routine monitoring of the composition and mass concentrations of ambient aerosol. Aerosol Sci. Technol. 45, 780–794. https://doi.org/10.1080/02786826.2011.560211

Ovadnevaite, J., Ceburnis, D., Canagaratna, M., Berresheim, H., Bialek, J., Martucci, G., Worsnop, D.R., O'Dowd, C. (2012). On the effect of wind speed on submicron sea salt mass concentrations and source fluxes. J. Geophys. Res. 117, D16201. https://doi.org/10.1029/2011JD017379

Paatero, P., Tapper, U. (1994). Positive matrix factorization: A non-negative factor model with optimal utilization of error estimates of data values. Environmetrics 5, 111–126. https://doi.org/10.1002/env.3170050203

Petit, J.E., Dupont, J.C., Favez, O., Gros, V., Zhang, Y., Sciare, J., Simon, L., Truong, F., Bonnaire, N., Amodeo, T., Vautard, R. (2021). Response of atmospheric composition to COVID-19 lockdown measures during spring in the Paris region (France). Atmos. Chem. Phys. 21, 17167–17183. https://doi.org/10.5194/acp-21-17167-2021

Safai, P.D., Raju, M.P., Rao, P.S.P., Pandithurai, G. (2014). Characterization of carbonaceous aerosols over the urban tropical location and a new approach to evaluate their climatic importance. Atmos. Environ. 92, 493–500. https://doi.org/10.1016/j.atmosenv.2014.04.055

Salcedo, D., Onasch, T.B., Aiken, A.C., Williams, L.D., De Foy, B., Cubison, M.J., Worsnop, D.R., Molina, L.T., Jimenez, J.L. (2010). Determination of particulate lead using aerosol mass spectrometry: MILAGRO/MCMA-2006 observations. Atmos. Chem. Phys. 10, 5371–5389. https://doi.org/10.5194/acp-10-5371-2010

Schaap, M., Otjes, R.P., Weijers, E.P. (2011). Illustrating the benefit of using hourly monitoring data on secondary inorganic aerosol and its precursors for model evaluation. Atmos. Chem. Phys. 11, 11041–11053. https://doi.org/10.5194/acp-11-11041-2011

Seinfeld, J.H., Pandis, S.N., Noone, K. (1998). Atmospheric chemistry and physics: From air pollution to climate change. Phys. Today 51, 88–90. https://doi.org/10.1063/1.882420

Sharma, V.K., Jinadatha, C., Lichtfouse, E. (2020). Environmental chemistry is most relevant to study coronavirus pandemics. Environ. Chem. Lett. 18, 993–996. https://doi.org/10.1007/s10311-020-01017-6

Simoneit, B.R., Schauer, J.J., Nolte, C.G., Oros, D.R., Elias, V.O., Fraser, M.P., Rogge, W.F., Cass, G.R. (1999). Levoglucosan, a tracer for cellulose in biomass burning and atmospheric particles. Atmos. Environ. 33, 173–182. https://doi.org/10.1016/S1352-2310(98)00145-9

Singh, V., Singh, S., Biswal, A., Kesarkar, A.P., Mor, S., Ravindra, K. (2020). Diurnal and temporal changes in air pollution during COVID-19 strict lockdown over different regions of India. Environ. Pollut. 266, 115368. https://doi.org/10.1016/j.envpol.2020.115368

Stohl, A. (1996). Trajectory statistics-a new method to establish source-receptor relationships of

air pollutants and its application to the transport of particulate sulfate in Europe. Atmos. Environ. 30, 579–587. https://doi.org/10.1016/1352-2310(95)00314-2

Sun, Y., He, Y., Kuang, Y., Xu, W., Song, S., Ma, N., Tao, J., Cheng, P., Wu, C., Su, H., Cheng, Y. (2020). Chemical differences between PM_1 and $PM_{2.5}$ in highly polluted environment and implications in air pollution studies. Geophys. Res. Lett. 47, e2019GL086288. https://doi.org/10.1029/2019GL086288

ten Brink, H., Otjes, R., Jongejan, P., Slanina, S. (2007). An instrument for semi-continuous monitoring of the size-distribution of nitrate, ammonium, sulphate and chloride in aerosol. Atmos. Environ. 41, 2768–2779. https://doi.org/10.1016/j.atmosenv.2006.11.041

Ulbrich, I.M., Canagaratna, M.R., Zhang, Q., Worsnop, D.R., Jimenez, J.L. (2009). Interpretation of organic components from positive matrix factorization of aerosol mass spectrometric data. Atmos. Chem. Phys. 9, 2891–2918. https://doi.org/10.5194/acp-9-2891-2009

Venter, Z.S., Aunan, K., Chowdhury, S., Lelieveld, J. (2020). COVID-19 lockdowns cause global air pollution declines. PNAS, 117, 18984–18990. https://doi.org/10.1073/pnas.2006853117

Via, M., Chen, G., Canonaco, F., Daellenbach, K.R., Chazeau, B., Chebaicheb, H., Jiang, J., Keernik, H., Lin, C., Marchand, N., Marin, C., O'Dowd, C., Ovadnevaite, J., Petit, J.E., Pikridas, M., Riffault, V., Sciare, J., Slowik, J.G., Simon, L., Vasilescu, J., *et al.* (2022). Rolling vs. seasonal PMF: Real-world multi-site and synthetic dataset comparison. Atmos. Meas. Tech. 15, 5479–5495. https://doi.org/10.5194/amt-15-5479-2022

Vinoj, V., Satheesh, S.K., Moorthy, K.K. (2010). Optical, radiative, and source characteristics of aerosols at Minicoy, a remote island in the southern Arabian Sea. J. Geophys. Res. 115, D01201. https://doi.org/10.1029/2009JD011810

Wang, P., Chen, K., Zhu, S., Wang, P., Zhang, H. (2020). Severe air pollution events not avoided by reduced anthropogenic activities during COVID-19 outbreak. Resour. Conserv. Recycl. 158, 104814. https://doi.org/10.1016/j.resconrec.2020.104814

Zhang, Q., Canagaratna, M.R., Jayne, J.T., Worsnop, D.R., Jimenez, J.L. (2005). Time- and size-resolved chemical composition of submicron particles in Pittsburgh: Implications for aerosol sources and processes. J. Geophys. Res. 110, D07S09. https://doi.org/10.1029/2004JD004649

Zhang, Q., Jimenez, J.L., Canagaratna, M.R., Allan, J.D., Coe, H., Ulbrich, I., Alfarra, M.R., Takami, A., Middlebrook, A.M., Sun, Y.L., Dzepina, K. (2007). Ubiquity and dominance of oxygenated species in organic aerosols in anthropogenically-influenced Northern Hemisphere midlatitudes. Geophys. Res. Lett. 34, L13801. https://doi.org/10.1029/2007GL029979

Zhang, Q., Jimenez, J.L., Canagaratna, M.R., Ulbrich, I.M., Ng, N.L., Worsnop, D.R., Sun, Y. (2011). Understanding atmospheric organic aerosols via factor analysis of aerosol mass spectrometry: A review. Anal. Bioanal. Chem. 401, 3045–3067. https://doi.org/10.1007/s00216-011-5355-y